

RECENT ADVANCES IN MAGNETIC RESONANCE MICROSCOPY TO THE PHYSICAL STRUCTURE CHARACTERIZATION OF CARBONACEOUS AND INORGANIC MATERIALS**

D. M. Gregory, R. E. Gerald, G. D. Cody and R. E. Botto
Chemistry Division
Argonne National Laboratory
9700 South Cass Avenue, Argonne, IL 60439

Abstract

Magnetic resonance microscopy (MRM) techniques have been employed to study the molecular architectures and properties of structural polymers, fossil fuels, microporous carbons and inorganic catalysts.

Keywords: solid state NMR, imaging, microscopy, materials

INTRODUCTION

In recent years, the field of magnetic resonance microscopy (MRM) has been advanced by the introduction of several new experimental techniques for the study of materials [1]. Our research has focused on specific methods that facilitate proton MRM of rigid solids, by utilizing proton multipulse line-narrowing in the presence of high gradient fields [2]. We have also developed new chemical-shift imaging strategies, which have been devised to highlight specific chemistries. We have used these techniques to investigate molecular transport of solvents and gases within polymers, catalysts and coals. Time-sequenced imaging of solvent uptake within macromolecular solids have been used to differentiate between Fickian and anomalous, or Case II, transport processes, analytical solutions to which form the basis of a model yielding information on the nature of transport in these systems, and ultimately, on their molecular architecture [3]. Current research in our laboratory is focussed on MRM to monitor porosities, pore-size distributions and diffusivities of methane and other gases in inorganic catalysts and high surface-area carbons.

In this paper, we highlight three recent developments in our laboratory: Applications to the areas of porosity measurements and the characterization of polymeric materials will be presented.

EXPERIMENTAL

Samples

A porous ceramic catalyst sphere (brand X) approximately 1.6 mm in diameter was prepared by immersing in water for several hours prior to the imaging experiment. The treated sample was then placed in a sealed teflon tube for imaging; the specimen contained 3.2 mg of water or the equivalent of about 10^{20} proton spins. The polymethylsilicone rubber sample was rectangular with initial dimensions of 2 x 2 x 1 mm, and the upper and lower sample surfaces protected from solvent infiltration by glass cover slips.

For chemical-shift imaging experiments, a test phantom was assembled from two concentric tubes: a 5-mm NMR tube was placed inside a 10-mm NMR tube. The inner tube contained acetone ($^1\text{H} \delta_B = 2.1$ ppm) and the annular region contained chloroform ($^1\text{H} \delta_A = 7.3$ ppm). A small amount of relaxation agent added to each solvent reduced the spin-lattice relaxation times by approximately one order of magnitude. The values of τ_{null}^A and τ_{null}^B were determined in a separate experiment by the inversion recovery method and found to be 35 and 50 ms, respectively.

MRM System and Experimentation

The MRM experiments were implemented on a portable, home-built Tecmag system operating at a proton Larmor frequency of 100.2 MHz. The system is capable of operating at frequencies between 50 and 400 MHz. Spectrometer control and data processing were executed by the software program MacNMR operating on a Macintosh Quadra 950 host computer.

The imaging probe having an outside diameter of 70 mm was constructed to fit within the room temperature shim stack of a wide-bore (89-mm) 2.35 T superconducting magnet, and could accommodate samples up to 28-mm in diameter. The design included rf coils for excitation and detection of the nuclear signals, and a set of gradient coils to create orthogonal gradient fields with respect to the three spatial coordinates. To maximize the filling factor of the rf coil and allow for different samples shapes, various coil and resonating structures ranging in diameter from 3-mm to 25-mm were interfaced to the probe. The probe was force-air cooled and was capable of operating with duty cycles in excess of 20% while producing a highly linear magnetic field gradient of up to 58 G/cm over a volume 30 mm in diameter.

MRM experiments were performed on the spherical catalyst specimen using 256 complex data points and a total of 3600 projections (30 θ angles over $\pi/2$ radians \times 120 ϕ angles over 2π radians). A gradient field of 25 G/cm and a sweep width of 60 kHz were employed. A total of 16 scans were collected for each projection using a 90°-pulse width (4- μ s duration) and a recycle delay time of 1 s, resulting in a total acquisition time of 16 hr.

In order to obtain sufficiently high quality images on the polymethylsilicone rubber specimen, it was necessary to acquire 32 (128 point) transients with a recycle delay of 500 ms for each of 128 phase-encoded gradient positions using a standard imaging spin-echo pulse sequence. This yielded a resolution on the order of 70 μ m, which was obtained over intervals of approximately 30 min. Typically a 64-kHz spectral width was chosen, establishing an echo time of 0.5 ms. Signal-to-noise improvement for the series of phase encoded echos was accomplished by apodization using a biexponential weighting function developed within the Macro subroutine of MacNMR.

RESULTS AND DISCUSSION

Determination of Porosity of Catalysts

In the first application, we have explored the potential of MRM to further the development of advanced formed absorbents and heterogeneous catalyst materials. Formed absorbents and catalyst systems on porous oxide supports are currently in use and are continually being improved in applications involving the production of upgraded hydrocarbon fuels or specialty chemicals. A detailed knowledge of the spatial distribution of the pore network is essential to the evaluation and improvement of catalyst and absorbent performance. MRM, utilizing filler fluids, offers the potential of spatially mapping the porosity of a variety of porous media. With application to spent catalysts, imaging techniques can be utilized to study the chemistry of catalyst coking, and has the ability to detect the spatial distributions of coke and other agglomerates in the pore matrix.

Figure 1 shows sequential 3D surface-rendered images with 20- μ m thick 2D slices displayed of internal portions throughout the catalyst sphere. The MRM experiment required a total of 3600 projections, or about 16 hr. for data acquisition. In this manner, an image resolution of 20 μ m was attained in each of the three spatial dimensions. Some thirty-two 2D image projections of proton spin density (where spin density scales linearly with image brightness) were used to provide estimates of total porosity and spatial distributions of pores throughout the specimen.

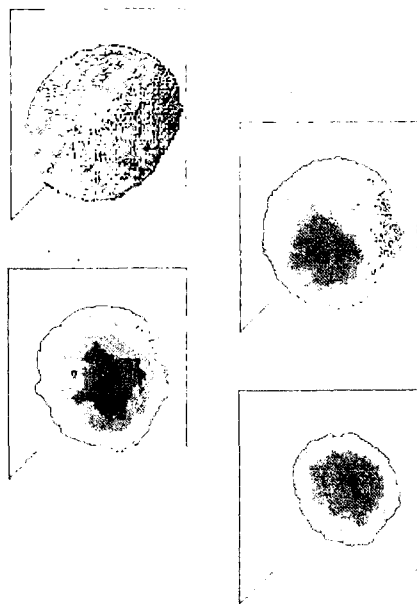


Figure 1. Three-dimensional MRM images of catalyst sphere.

Performing MRM experiments on the catalyst sphere presents the opportunity to discuss the limits of resolution in image reconstruction, on a sample for which the spectral resolution of individual projections is very high ($< 1 \mu\text{m}$) because of its inherently narrow proton linewidth. For example, given our catalyst sample of maximum radius equal to 0.8 mm (a diameter of 1.6 mm), the total number of projections required to obtain an image having a resolution of $20 \mu\text{m}$ is calculated to be 10,953. If lower resolution can be tolerated in the resultant images, the number of projections becomes even more reasonable. In order to achieve a resolution of $40 \mu\text{m}$, for example, the number of projections required is only 3,943. In practice, these numbers can be reduced by a factor of two or three if one employs significant filtering in the reconstruction algorithm. Thus, acquiring 3600 projections for our catalyst specimen is sufficient to achieve the desired resolution provided that appropriate filtering is applied. Finding that an adequate SNR ratio for each projection can be attained in 16 acquisitions employing a 1 s pulse repetition time translates into a total experimental averaging time of about 16 hr.

^{19}F MRM of Solvent Transport In Rubbers

Significant insight into the character of solvent transport has been obtained through time-resolved, ^{19}F NMR imaging of solvent concentration and network dilation changes that occur during solvent uptake within rubbery polymer networks. Complications found in proton NMR imaging experiments, because contributions to the signal intensity can arise from both the protons of the solvent and protons of the mobile polymer backbone, can be averted using fluorinated solvents. In the present study, ^{19}F imaging has been employed to investigate Fickian transport of hexafluorobenzene within a specimen of polymethylsilicone (PMS) rubber.

Sequential 2D ^{19}F images of a specimen of PMS swelling in hexafluorobenzene, observed at early (top), intermediate (middle) and advanced (bottom) solvent diffusion times are shown in Figure 2. Clearly evident is the smooth, exponential, solvent gradients directed into the core of the sample, indicating a Fickian transport mechanism.

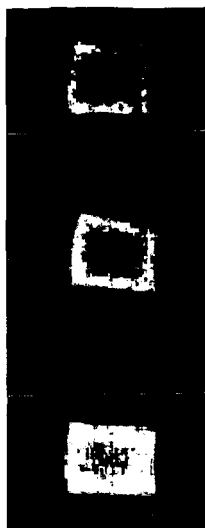


Figure 2. Sequential ^{19}F images of hexafluorobenzene transport in polymethylsilicone.

The measured front velocities from MRM provide a valuable and quantitative constraint for the parameterization of the uptake data. Direct measurement of linear dilation accompanying swelling is a simple means to quantify the overall swelling behavior of rubbery networks. Linear dilation behavior for PMS was consistent with Fickian transport in rubbery networks. Given the uptake data, it was trivial to derive a mass-fixed diffusion coefficient through linear fitting of the experimental data. The generation of a curve for Fickian transport, in the present case, requires solving the two-dimensional diffusion equation and integrating this solution with respect to time. Fitting of the dilation data results in values of $D_R = 1.1 \times 10^{-6} \text{ cm}^2/\text{s}$ for PMS-hexafluorobenzene. These relatively large values of D_R reflect the high degree of inter- and intra-molecular mobility of the network, which explains the rapidity with which the rubbery systems respond to applied stresses that are osmotic in nature.

Chemical-Shift MRM of Binary Systems

In this last section, we present a new method for chemical-shift selective MRM, selective-echo chemical-shift imaging (SECSI), which is easily implemented and can be executed in a short time period ($<1 \text{ ms}$). The SECSI pulse sequence is designed to select the magnetization from one of two chemical species. Subsequently, this magnetization is used to form a spin-echo in the conventional manner. The magnetization of the second chemical species is initially placed antiparallel to the Zeeman field and is then allowed to decay to zero via T_1 relaxation; therefore, it does not contribute

to the spin-echo. In the simplest case, each chemical species is represented by a single NMR resonance; however, a cluster of closely spaced resonances for each species is also suitable for NMR imaging by the SECSI method. The full Boltzmann magnetization is used for imaging either chemical species; this approach presents an advantage over many other pulse methods. Both chemical species can have any value for T_1 and concentration. Additionally, the method employs only hard pulses of quadrature phase and is easily implemented using standard spectrometer hardware.

The SECSI pulse sequence is a *chemical-shift filter* consisting of two 90° pulses and two delays $(90^\circ_x - \tau_{\text{antiphase}} - 90^\circ_x - \tau_{\text{null}})$ and is executed prior to a standard spin-echo imaging sequence [4]. The RF transmitter is centered on one of the NMR resonances of a two-component system A and B where $\delta_A > \delta_B$. In a reference frame rotating (clockwise) at ω_A (component A on resonance), the magnetization vector for the A spins is stationary, while the magnetization vector for the B spins precesses (counterclockwise) at $\omega_A - \omega_B$. The initial 90°_x pulse tips the magnetization of both components on to the $+y$ axis in the xy -plane. An antiphase period, $\tau_{\text{antiphase}}$, equal to $\pi/(\omega_A - \omega_B)$ is allowed to elapse such that the magnetization vectors from both components become mutually out of phase by 180° . The second pulse, 90°_{-x} , restores the Boltzmann magnetization of component A along the $+z$ axis while inverting the spin population of component B . After an inversion recovery delay, τ_{null}^B , equal to $\ln 2 T_1^B$, the only net z magnetization remaining is that of component A (restored along the $+z$ axis following the second RF pulse). At this point a standard 2D spin-echo imaging pulse sequence is executed, which yields the chemical-shift selective image of component A . The complementary image, the chemical-shift selective image of component B , is obtained by placing component B on resonance and repeating the pulse sequence. The antiphase period remains the same, however, the inversion recovery delay in this case is set to τ_{null}^A , given by $\ln 2 T_1^A$.

The antiphase period, $\tau_{\text{antiphase}}$, defines the duration of the transverse spin evolution within the pulse sequence and, therefore, the time during which T_2^* processes play a role in diminishing the final signal intensity. A general expression for the antiphase period is given by

$$\tau_{\text{antiphase}} = \frac{\pi \times 10^6}{\Delta \gamma_N B_0} \quad [1]$$

where Δ is the separation between the two resonances in parts per million ($\Delta = \delta_A - \delta_B$), γ_N is the gyromagnetic ratio of the nuclear spins (2.67506×10^8 rad $T^{-1} \cdot s^{-1}$ for 1H), and B_0 is the external magnetic field strength. The antiphase period decreases monotonically for higher field strengths. For systems in which the bandwidths of the resonances are inhomogeneously broadened, the inversion recovery delay following the antiphase period serves a second purpose. Following the second RF pulse, any off-resonance contribution to the magnetization of the species returned to the $+z$ axis will not have been returned completely to the Boltzmann equilibrium position. Therefore, during the inversion recovery delay this off-resonance magnetization recovers towards Boltzmann equilibrium. This added feature of the pulse sequence compensates for effects of the antiphase period, during which the net magnetization may be reduced by the inhomogeneity of the magnetic field, a dispersion of chemical shifts, and spin-spin relaxation.

Figure 3 represents a proton 2D NMR image of the phantom that was acquired by using the conventional spin-echo imaging technique. The central region of this image appears brighter because of the greater concentration of protons in acetone; the proton concentration ratio is 6.54 : 1.00 for acetone vs. chloroform. Although the large difference in proton concentrations provides substantial contrast between the two solutions, one cannot determine from the image alone which regions represent chloroform or acetone *a priori*. The SECSI method was used to selectively image the protons of acetone at $^1\text{H}\delta_b = 2.1$ ppm (Fig. 3b) and the protons of chloroform at $^1\text{H}\delta_a = 7.3$ ppm (Fig. 3c). In images 3b and 3c there is no ambiguity as to what the bright regions represent, and no inference is necessary to describe the spatial distribution of either chemical species. Furthermore, note the large dynamic range obtained for suppressing the image intensity of the unwanted magnetization.

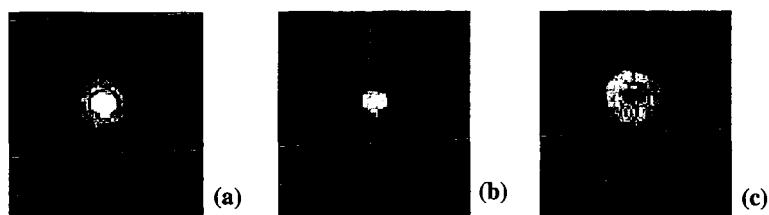


Figure 3. Proton MRM images of acetone-chloroform phantom: (a) conventional 2D spin-echo image; (b) chemical-shift selective image of acetone in the 5 mm NMR tube; (c) chemical-shift selective image of chloroform in the annular region between the 5 and 10 mm NMR tubes.

For systems containing three NMR resonances, representing different chemical species, the SECSI sequence may be applied sequentially to preferentially select one of the chemical species for imaging. The method requires phase cycling to cancel interfering transverse magnetization and can only be executed optimally for certain ratios of the T_1 's. Simultaneous selective excitation and subsequent imaging of two groups of resonances in a complex ^{19}F NMR spectrum was effectively demonstrated by Börnert and coworkers [5]. For the ubiquitous cases of water/fat or water/oil systems the SECSI technique offers simplicity, fast execution, and the highest sensitivity.

ACKNOWLEDGMENT

This work was performed under the auspices of the Office of Basic Energy Sciences, Division of Chemical Sciences, U. S. Department of Energy, under Contract No. W-31-109-ENG-38.

REFERENCES

1. "MRI of Materials", R. E. Botto, Ed., *Solid State NMR*, **6**, No. 4 (1996).
2. S. L. Dieckman, P. Rizo, N. Gopalsami, J. P. Heeschen and R. E. Botto, *J. Am. Chem. Soc.*, **114**, 2717 (1992).
3. G. C. Cody and R. E. Botto, *Energy Fuels*, **7**, 561 (1993).
4. S. L. Talagala and I. J. Lowe, *Concepts Magn. Reson.* **3**, 145-159 (1991).
5. P. Börnert, W. Dreher, A. Gössler, G. Klee, R. Peter, and W. Schneider, *J. Magn. Reson.* **81**, 167-172 (1989).